


Retrogressive thaw slump susceptibility in the northern hemisphere permafrost region

Eirini Makopoulou¹  | Olli Karjalainen¹ | Letizia Elia² | Andrée Blais-Stevens³ | Trevor Lantz⁴ | Panya Lipovsky⁵ | Luigi Lombardo⁶ | Ionut C. Nicu⁷ | Lena Rubensdotter^{8,9} | Ashley C. A. Rudy¹⁰ | Jan Hjort¹

¹Geography Research Unit, University of Oulu, Oulu, Finland

²Department of Physics and Astronomy, University of Bologna, Bologna, Italy

³Natural Resources Canada, Geological Survey of Canada, Ottawa, Canada

⁴School of Environmental Studies, University of Victoria, Victoria, British Columbia, Canada

⁵Yukon Geological Survey, Government of Yukon, Whitehorse, YT, Canada

⁶University of Twente, Faculty of Geo-Information Science and Earth Observation (ITC), Enschede, the Netherlands

⁷High North Department, Norwegian Institute for Cultural Heritage Research (NIKU), Tromsø, Norway

⁸Geological Survey of Norway (NGU), Trondheim, Norway

⁹Arctic Geology Department, The University Centre in Svalbard (UNIS), Longyearbyen, Norway

¹⁰Northwest Territories Geological Survey, Government of the Northwest Territories, Yellowknife, NT, Canada

Correspondence

Eirini Makopoulou, Geography Research Unit, University of Oulu, Oulu, 90014, Finland.
Email: eirini.makopoulou@oulu.fi

Funding information

Kvantum Institute, University of Oulu; Research Council of Finland, Grant/Award Number: 315519

Abstract

Mean annual temperatures in the Arctic and subarctic have increased in recent decades, increasing the number of permafrost hazards. Retrogressive thaw slumps (RTSs), triggered by the thawing of ground ice in permafrost soil, have become more common in the Arctic. Many studies report an increase in RTS activity on a local or regional scale. In this study, the primary goals are to: (i) examine the spatial patterns of the RTS occurrences across the circumpolar permafrost region, (ii) assess the environmental factors associated with their occurrence and (iii) create the first susceptibility map for RTS occurrence across the Northern Hemisphere. Based on our results, we predicted high RTS susceptibility in the continuous permafrost regions above the 60th latitude, especially in northern Alaska, north-western Canada, the Yamal Peninsula, eastern Russia and the Qinghai-Tibetan Plateau. The model indicated that air temperature and soil properties are the most critical environmental factors for the occurrence of RTSs on a circumpolar scale. Especially, the climatic conditions of thaw season were highlighted. This study provided new insights into the circumpolar susceptibility of ice-rich permafrost soils to rapid permafrost-related hazards like RTSs and the associated impacts on landscape evolution, infrastructure, hydrology and carbon fluxes that contribute to global warming.

KEYWORDS

circumpolar susceptibility, mass-movements, permafrost degradation, retrogressive thaw slumps, statistical modelling, Thermokarst

1 | INTRODUCTION

In recent decades, mean annual air temperatures in the Arctic and subarctic have increased 2–4 times faster than the global average rate, and warming is likely to continue at faster rates in the current century (IPCC, 2021; Rantanen et al., 2022; Snyder, 2016). Permafrost is defined as ground (soil and rock) that remains at or below 0°C for at least two consecutive years (Brown, Sidlauskas, & Delinski, 1997). Since 1980, monitoring the thermal state of permafrost has provided

clear evidence of warming and thawing throughout permafrost regions (Biskaborn et al., 2019; Harris et al., 2009; Pastick et al., 2015; Romanovsky, Smith, & Christiansen, 2010; Smith et al., 2022; Wang et al., 2015). However, permafrost degradation increasingly occurs also in areas of cold permafrost. Rising ground temperatures have been associated with increases in the frequency and intensity of disturbance associated with thawing permafrost (Fraser et al., 2018; Lewkowicz & Way, 2019; Nitze et al., 2020). The potential impacts of permafrost thaw are most significant in areas with high ground

This is an open access article under the terms of the [Creative Commons Attribution](https://creativecommons.org/licenses/by/4.0/) License, which permits use, distribution and reproduction in any medium, provided the original work is properly cited.

© 2024 The Author(s). *Earth Surface Processes and Landforms* published by John Wiley & Sons Ltd.

ice content. The thawing of ice-rich permafrost can affect local landscapes, ecosystems and the global climate due to the release of soil carbon into the atmosphere (Kokelj & Jorgenson, 2013; Turetsky et al., 2020).

Permafrost thaw-related hazards have been studied across the Arctic from local to regional scales by Bartleman et al. (2001), Lantz et al. (2009), Jones, Pollard, & Jones (2019) and Nitze et al. (2020). One of the most common permafrost hazards is retrogressive thaw slumps (RTSs) (Figure 1). RTSs form on destabilized slopes that have been affected by mass wasting, erosion, wave action, wildfires or other activities that lead to the exposure and melt of ground ice. This results in the collapse of the thawed soil and the initiation of RTS (Burn & Lewkowicz, 1990). RTSs involve soil movement and

vegetation displacement, which result in a large scar area (a horseshoe or a bowl-shaped depression with a steep headwall) (Huebner & Bret-Harte, 2019). RTSs are characterized by the exposure of ground ice in ice-bearing permafrost deposits, and they are one of the most dynamic thermokarst landforms in the Arctic (Bernhard et al., 2020; Malone et al., 2013). They usually occur on slopes with fine-grained ice-rich sediments (Lacelle, Bjornson, & Lauriol, 2010), and many are found along rivers, lakeshores or coastal bluffs, where coastal or fluvial processes provide the initial slope and exposure for permafrost to thaw (Swanson, 2014). Previous studies have pointed out that RTSs occur primarily after warm and rainy summers due to the deep active layer thaw in permafrost soils (Burn & Lewkowicz, 1990; Kokelj, Tunncliffe, Lacelle, Lantz, Chin, & Fraser, 2015; Lewkowicz &

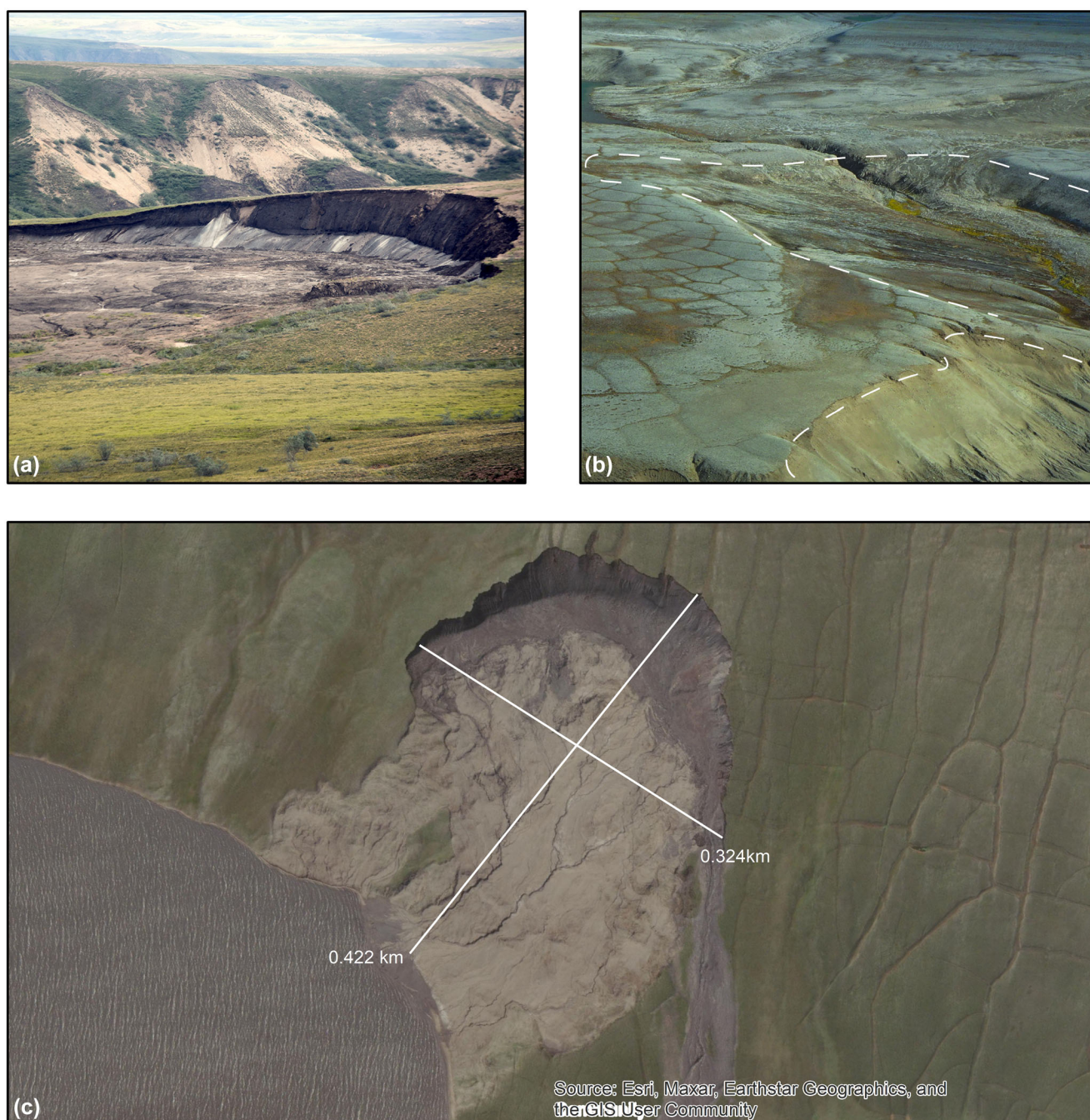


FIGURE 1 a) Retrogressive thaw slump (RTS) in Paulatuk region, Northwest Territories, Canada, (photo: Trevor Lantz) b) RTS located near the bank of Linnéelva River, close to Russekeila, Svalbard. The hatched lines show back-scarps (photo: Lena Rubensdotter), and c) RTS on Banks Island, Canada.

Way, 2019). Once RTSs are initiated, they may continue to develop for many years, and at some sites, growth may continue for decades (Burn & Lewkowicz, 1990). Segal, Lantz, & Kokelj (2016) and Lewkowicz & Way (2019) have pointed out the rapid intensification of slumps in recent decades and suggested that climatic and terrain factors are important influences.

Retrogressive thaw slumps tend to occur in clusters, and it is not uncommon to find several in a small area (Jones, Pollard, & Jones, 2019). RTSs are local permafrost hazards, but when present in high concentrations, they can affect geomorphology, hydrology, ecology, Arctic infrastructure development and biogeochemistry from local to regional scales (Hjort et al., 2022; Kokelj et al., 2021; Nitze et al., 2018; Patton, Rathburn, & Capps, 2019). RTSs disrupt the surface organic cover and promote seral vegetation adapted to warmer and less organic soils (some herbs and deciduous shrubs) at the expense of evergreen shrubs, lichens, some mosses (Bartleman et al., 2001) and alder growth (Lantz et al., 2009). Additionally, RTS formation exposes soil organic matter to degradation and thus increases carbon fluxes that contribute to global warming (Ramage et al., 2018; Turetsky et al., 2020).

The distribution of RTSs has previously been modelled only at local and regional scales (e.g., Rudy et al., 2016; Yin et al., 2021), and broad-scale assessments are lacking. Consequently, the spatial and temporal characteristics of RTS occurrence are still unclear, and a more thorough evaluation of the factors controlling landscape sensitivity to thaw slumps is required. To address this, we integrate previous and new information on the circumpolar distribution of RTSs and use these data (i) to study the spatial patterns of the occurrence of RTSs across the circumpolar permafrost region, (ii) to assess the

environmental factors that are related to their occurrence and (iii) to create the first susceptibility map for RTS occurrence across the Northern Hemisphere. We use statistical modelling techniques to correlate an extensive dataset of confirmed RTS occurrences to high-resolution geospatial data on relevant environmental conditions and predict the susceptibility of RTS occurrence in the Northern Hemisphere.

Our combined results thus supply information about the environmental factors that control the susceptibility of RTS occurrences and provide new spatial insights into the susceptibility of circumpolar permafrost to RTS development.

2 | DATA AND METHODS

2.1 | RTS inventory

RTS observations ($n = 19,227$, see Supplementary material), across the permafrost region (Figure 2) were compiled from published inventories in online databases and articles and by visual interpretation of the Arctic Imagery (ESRI, 2020) with a 15-m resolution for the circumpolar region in the ArcGIS Pro software (version 3.1.0). The Arctic imagery was chosen because of its consistent availability, especially for the previously unmapped Siberian coast (Sakha region), where visual interpretation was performed to fill gaps in circumpolar data coverage.

The dual-observe approach was applied for the visual interpretation, where first, authors (EM and LE) identified RTSs according to their morphologic characteristics (e.g., shape and scar zone). To

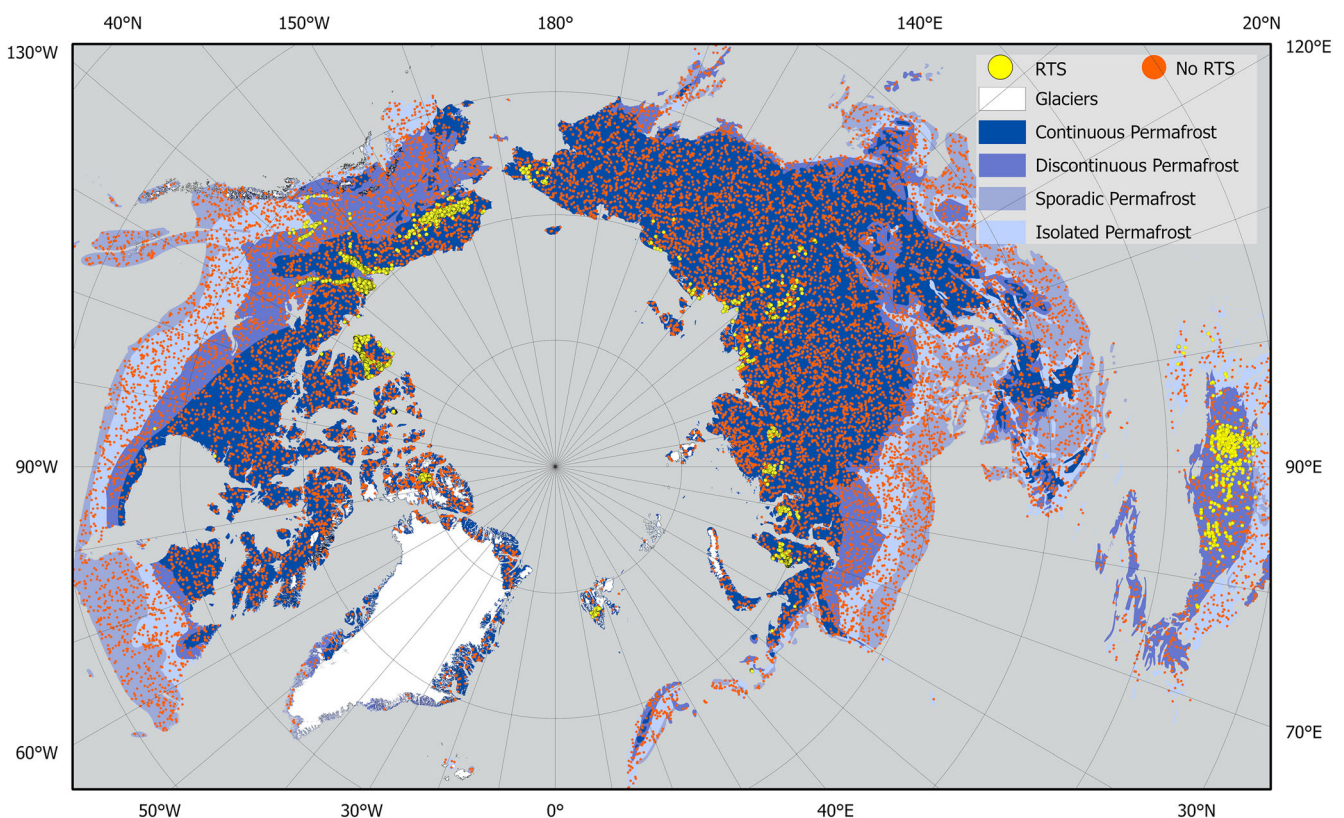


FIGURE 2 Distribution of the compiled retrogressive thaw slumps $n = 19,227$ (RTS) and non RTS across the permafrost region (permafrost zones based on Brown, Sidlauskas, & Delinski, 1997).

achieve a homogenous dataset over a vast area, a standardized criterion was that mapped RTSs should be visible at a scale of 1:10,000. Second, the final RTS dataset was reviewed by the author (EM). Most of the observations in the literature and databases were originally mapped between 1980 and 2020, with few exceptions from the 1950s. The observations that were in polygon shapefiles were converted to points with the tool Feature To Point in ArcGIS Pro based on polygon centroid.

To facilitate presence-absence modelling (see Figure 2), a random sample of absences (non-RTS) was drawn from inside the Brown, Sidlauskas, & Delinski (1997) permafrost region (all permafrost zones). First, a random sample of 17,000 points was created in ArcGIS Pro at a minimum distance of 1,000 m from each other and from the presence points. This distance is meant to ensure that locations potentially associated with presence instances do not enter the model and act as noise in the classification process. This procedure was further refined in a subsequent step, where fine-resolution satellite imagery in ArcGIS Pro was employed to verify that no RTSs were present in the vicinity (500 m search radius) of the sampled locations. To avoid pseudo-replication, we ensured that each 30-arc-second ($\sim 1 \text{ km}^2$) grid cell containing more than one observed RTS was only used once in the modelling (see section 2.3.1.). The dataset consisted of 28,931 30-arc-second ($\sim 1 \text{ km}^2$) grid cells (RTS-present = 11,931; and RTS-absent = 17,000).

2.2 | Environmental predictors

Several geospatial datasets with 30 arc-second spatial resolution were used to characterize environmental conditions affecting the circumpolar occurrence of RTSs. We performed preliminary modelling with different physically relevant data on topography, soil and climate variables to determine which parameters performed most robustly in spatial prediction. The investigated variables included soil conditions (Poggio et al., 2021; Shangquan et al., 2017), climate (Karger et al., 2017), topography (Amatulli et al., 2020), vegetation and ground ice conditions (Brown, Sidlauskas, & Delinski, 1997; Strauss et al., 2021). Based on pre-analysis, we excluded variables (see Supplementary Material Table S1) that had either an overly strong correlation with a similar variable (e.g., mean annual air temperature and thawing degree-days) or negligible effect in initial models. The final environmental variables selected for the modelling are shown in Table 1.

TABLE 1 The environmental predictors used in the modelling.

Environmental predictors	Source data	Reference
Thawing degree days (TDD, °C-days)	CHELSA Climate data	Karger et al., 2017
Freezing degree days (FDD, °C-days)	CHELSA Climate data	Karger et al., 2017
Rainfall (mm)	CHELSA Climate data	Karger et al., 2017
Slope angle (°)	Geomorpho90m	Amatulli et al., 2020
Fine sediment content (g/kg ¹)	SoilGrids250m 2.0	Poggio et al., 2021
Bulk density (bd, g/cm ³)	SoilGrids250m 2.0	Poggio et al., 2021

Climate variables were calculated for the climate normal period 1981–2010. Freezing and thawing degree days (FDD and TDD, °C-days) were calculated as the annual sums of monthly average temperatures below and above freezing, respectively. Following Aalto et al. (2018), rainfall was calculated as the annual sum of precipitation for months with an average air temperature over 0°C.

In addition to the climatic variables, one topographic variable (slope angle) and two soil variables (i.e., fine sediment [clay to silt fraction] content and dry bulk density of the soil) were also used in the susceptibility modelling. The mean of slope angle was computed using the Geomorpho90m dataset (resolution = 3 arc-second; $\sim 90 \text{ m}$) aggregated to the used 30 arc-second spatial resolution (Amatulli et al., 2020). Soil (unconsolidated sediment) properties are very important for RTS development because they affect the frost susceptibility, water transport capacity and hence indirectly the ground ice content of the sediments. In fine-grained materials, both frost susceptibility and ground ice content are typically higher than in coarse materials (e.g., Kokelj & Burn, 2005). Another soil property was bulk density, which was considered to account for the overall compactness of the soils. Low values indicate loose soils with abundant organic content, while high values are found in dense silty and clayey soils with less pore space (O'Connor et al., 2020). The soil variables were obtained from the SoilGrids250m 2.0 database with the definition that “soil” is up to 2 m thick unconsolidated material (Poggio et al., 2021). We computed average soil property values for the depth 0–200 cm based on the values provided for six depth intervals and aggregated the average of the original 7.5 arc-second data to 30 arc-second resolution.

2.3 | Statistical modelling

2.3.1 | Sampling design

The compiled RTS observations have a relatively large extent across the circumpolar area, yet in some regions, the RTSs are more clustered than in others. Such spatial structures in the modelling data can lead to overoptimistic estimates of model performance, e.g., in the case of unaccounted spatial autocorrelation (Schratz et al., 2019). On the other hand, randomly selected absences are evenly distributed. To control these different spatial structures and the likely strong spatial autocorrelation among the presences, a repeated distance-based random sampling was performed. Altogether, the models were run 10 times with different sub-samples in which spatial autocorrelation and the imbalance of sampled presences and absences were constrained (see below for details). This procedure ensures that any residual spatial structure in the data can be perturbed or even broken down to the point of removing its influence on model performance (e.g., Moreno et al., 2023).

At each modelling round, the *zerodist2* function in the R package *sp* (Pebesma, 2018) was used with a 2-km search distance to remove observations in adjacent grid cells in the entire dataset. Before these omissions were made, the dataset was shuffled to ensure that different samples were selected at each round. The rationale was to make the spatial structures of clustered presences and evenly distributed absences more similar. On average, roughly 19,700 observations remained at each round.

Next, *zerodist2* was used to randomly split the data into model calibration and evaluation datasets. At each round, random samples used for the model calibration datasets were drawn so that the observations were at least 10 km apart from the observations in the corresponding evaluation datasets. This procedure was performed to increase the spatial independence of calibration and evaluation datasets, which are crucial in validating the models' predictive performance outside of the spatial setting of the calibration data (Hao et al., 2020; Valavi et al., 2021). A relatively conservative distance was used so that this procedure did not omit too many of the identified RTSs. Initially, 90% of observations were randomly assigned as calibration data, and 10% were reserved for evaluation. By doing this, we aimed to use a maximum amount of data to train the models, and thus reduce the need to extrapolate the model outside the realized predictor space (Roberts et al., 2017). On average, 1,566 identified RTSs (presences) and 14,075 non-RTSs (absences) were selected at each of 10 sampling rounds to form calibration datasets, and an average of 358 presences and 1,600 absences were in evaluation datasets.

The apparent class imbalance in the obtained datasets (low prevalence of presences, Valavi et al., 2022) could decrease the predictive performance of modelling (Valavi et al., 2021, 2022) and produce artificially significant error estimates (Roberts et al., 2017). For this reason, an equal sampling was also performed (Brenning, 2005). The technique has been shown to improve prediction performance and reduce overfitting in statistically based modelling (Valavi et al., 2021) and in defining optimal threshold values to produce binary predictions (Liu et al., 2005; Zhang et al., 2019). In this procedure, an equal number of absences and presences were selected at each round in both calibration and evaluation datasets. The number of observations in both classes was equal to the presence in the random distance-based samples. Thus, on average, 3,200 presences and absences were used in the final model calibration and 670 presences and absences were retained for evaluation.

2.3.2 | Modelling techniques

The occurrence of RTSs was analysed using a generalized boosting model (GBM) with the BIOMOD2 package (Thuiller et al., 2009, version 3.5.1) in R Statistics software version 4.1.2 (R Core Team, 2022). GBM was selected based on preliminary analyses where commonly applied techniques (Aalto, Harrison, & Luoto, 2017; Aalto & Luoto, 2014; Karjalainen et al., 2020; Leppiniemi et al., 2023; Rudy et al., 2016; Yin et al., 2021), were compared based on evaluation metrics (see Figures S1-S3 and Table S2 in the supplementary material).

GBM is a machine learning method that combines many classification trees to form a model with improved prediction accuracy, which in some cases can address overfitting (Elith et al., 2005). With GBM, we used 5,000 trees, interaction depth = 5, shrinkage = 0.05 and bag fraction = 0.75. A sensitivity analysis was performed by testing a different maximum number of trees (1,000–8,000) and shrinkage values (0.005, 0.01 and 0.05), with the aim of finding optimal settings for the influence of individual trees in the final model (Elith, Leathwick, & Hastie, 2008). A relatively fast rate was found to yield the most balanced predictive performance.

To evaluate the overall performance of the model, the receiver operating curve (ROC) and true skill statistics (TSS) were implemented. ROC analysis is a common graphical approach for analysing the performance of a binary classifier, and it uses a pair of statistics – true positive rate and false positive rate – to characterize a classifier's performance (Tan, 2009). TSS is an accuracy measure that considers both omission and commission errors and success because of random guessing and ranges from -1 to $+1$, where $+1$ shows perfect agreement (Allouche, Tsoar, & Kadmon, 2006). For ROC and TSS, sensitivity and specificity values were also calculated. Sensitivity values are the percentage of presences correctly predicted in the model, and specificity values are the percentage of absences correctly predicted in the model (Guisan, Thuiller, & Zimmermann, 2017).

To examine the relative contributions of the environmental factors, the variable importance values were calculated. In addition, response curves for each predictor were computed to examine their effect on the predicted RTS probability. We normalized the predicted probabilities so that the values from each of the 10 runs were internally normalized between 0 and 1. The shape of the response curve is representative of the statistical relationship between the geomorphic process (RTS) and the predictor variable (environmental variables) when other variables are held constant (Hjort & Luoto, 2011).

2.3.3 | Susceptibility maps

To create the susceptibility map, we classified the predicted probabilities of RTS occurrence (the average of 10 model runs) into susceptibility zones using the 50th, 75th, 90th and 95th percentiles, which represent the areas with very low <50, low 50–75, medium >75–90, high >90–95 and very high >95 probability for future disturbance, similar to Goetz et al. (2015), Rudy et al. (2016) and Yin et al. (2021). The analysis is based on the assumption that areas that are predicted as susceptible to RTSs will have terrain conditions comparable to those in areas where RTSs have already occurred.

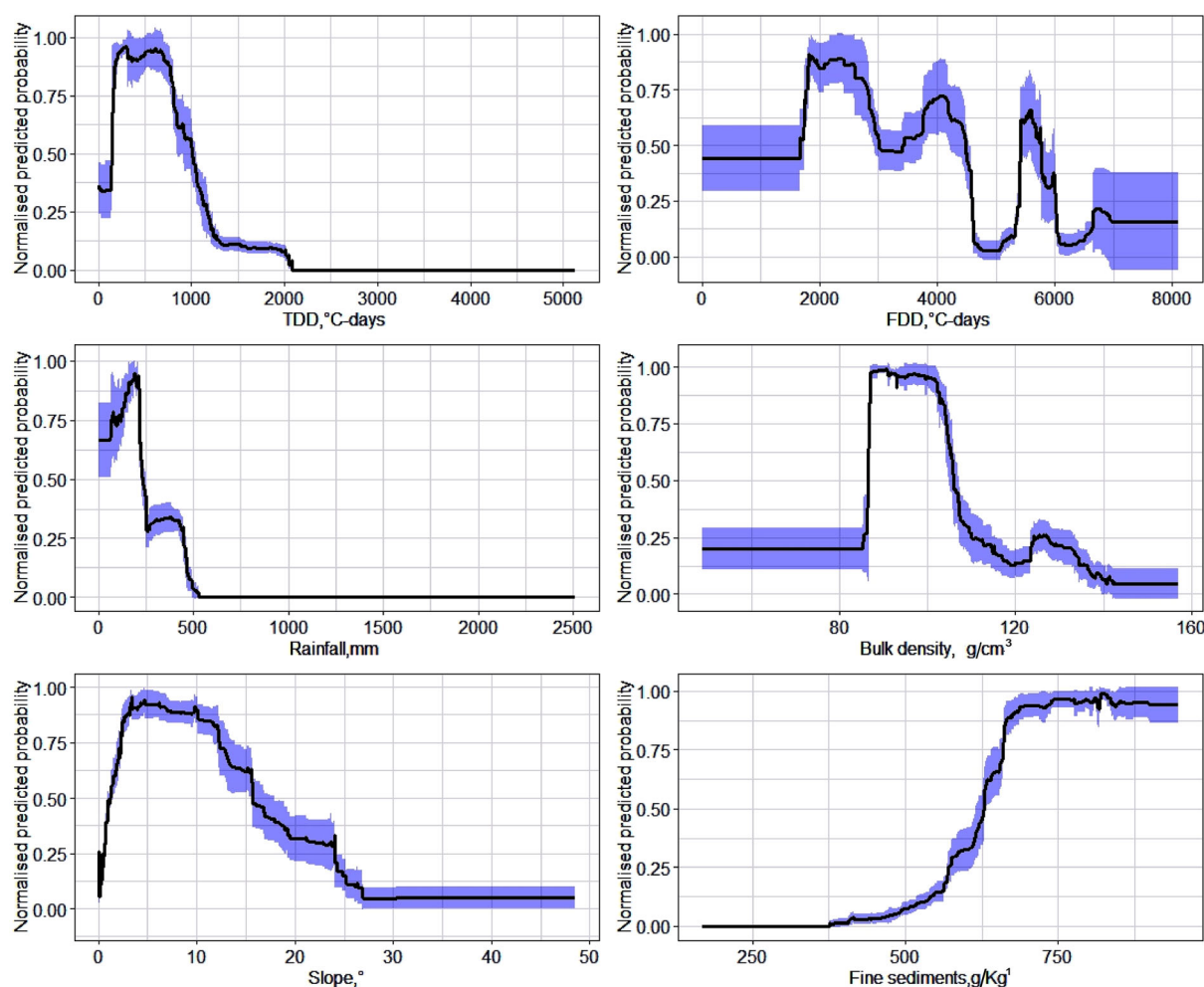
3 | RESULTS

3.1 | Environmental factors affecting RTSs occurrence

Based on the analysis of variable importance (Table 2), the most critical variables for the RTSs occurrence are TDD, FDD, rainfall and bulk density. The response curve for TDD (Figure 3) shows that the highest probability for RTS occurrence is found between approximately 100 and 1,100°C-days. In the case of FDD, the highest probabilities occur approximately between 1,900 and 5,800°C-days. Rainfall's response curve indicates optimal conditions where precipitation is below 500 mm, whereas the bulk density shows the highest probability within a quite narrow range between 90 and 105 g/cm³. The response curve for slope angle shows that RTSs are located most likely on slopes below 20°, but also that probability in completely flat areas as well as on steep slopes (>25°) is low. Additionally, the response curve for fine sediments shows that the RTSs occur where the fraction of fine sediments is above approximately 650 g/kg¹.

TABLE 2 Variable importance over 10 modelling runs for the generalized boosting model (GBM). The abbreviated predictors are freezing degree-days (FDD) and thawing degree-days (TDD).

GBM	TDD	FDD	Rainfall	Bulk density	Slope angle	Fine sediments
Average	0.41	0.33	0.20	0.17	0.11	0.07
Standard Deviation	0.03	0.02	0.02	0.03	0.04	0.01

**FIGURE 3** Response curves for the environmental variables used in the generalized boosting model. The thick black line represents the mean values over 10 model runs, and the blue band depicts one standard deviation above and below the mean. The abbreviated predictors are freezing degree-days (FDD), and thawing degree-days (TDD). Response curves for the auxiliary modelling methods used in the pre-analyses are presented in the supplementary material (Figures S4, S5 and S6).**TABLE 3** Statistical evaluation metrics for the receiver operating curve (ROC), true skill statistics (TSS), sensitivity and specificity for the training and evaluation datasets based on 10 modelling runs of the generalized boosting model (GBM).

	Training data		Evaluating data		Cutoff		Sensitivity %		Specificity %	
	ROC	TSS	ROC	TSS	ROC	TSS	ROC	TSS	ROC	TSS
GBM average	0.93	0.75	0.93	0.74	0.52	0.52	92.28	92.30	82.93	82.77
GBM Standard deviation	0.004	0.009	0.007	0.01	17.21	15.33	1.02	0.79	1.33	1.24

Based on the 10-fold distance-based random cross-validation, the trained GBM models showed robust predictive performance with spatially semi-independent evaluation datasets (Table 3). Prediction accuracy, as indicated by ROC and TSS values, was similar across training and evaluation data and showed a small

standard deviation across the 10 model runs. More specifically, the average sensitivity and specificity values show that the models correctly predicted the presence of RTS in the evaluation datasets in approximately 92% of cases and their absence in 83% of cases.

3.2 | Circumpolar susceptibility map

High RTS susceptibility was predicted extensively in the continuous permafrost regions, while discontinuous permafrost regions typically had low to very low susceptibility values. The most extensive areas of very high susceptibility were found across the Brooks Range in Alaska, the Northwest Territories of Canada (Banks Island, Victoria Island, parts of Ellesmere Island, Mackenzie Bay, Franklin Bay and Darnley Bay), North-western Passages show medium to high susceptibility in some parts of Baffin Island and Kativik territory, the eastern coasts of Greenland, Svalbard, Yuzhny Island, Yamal, Gydan and Taymyr Peninsulas, the northern Siberian coast and Chukotka Peninsula. Outside the Arctic, very high susceptibility was also predicted in the Qinghai-Tibetan Plateau (Figure 4a).

4 | DISCUSSION

With statistical modelling, we effectively identified key factors that have a significant impact on RTS activity, which can help to better understand their circumpolar distribution and the underlying causes of their occurrence (Elia et al., 2023). Our results showed that RTS occurrence at a circumpolar scale can be reasonably well predicted with climatic (FDD, TDD, rainfall), soil (bd and fine sediment fraction) and topographic (slope angle) variables. Interestingly, thaw-related variables (TDD and rainfall) were highlighted in the results and had more distinct thresholds when compared to FDD, thus showing the importance of summer conditions for the occurrence of RTSs (Mekonnen et al., 2021; Peng et al., 2018). Previous studies have shown similar results for RTSs at local and regional scales

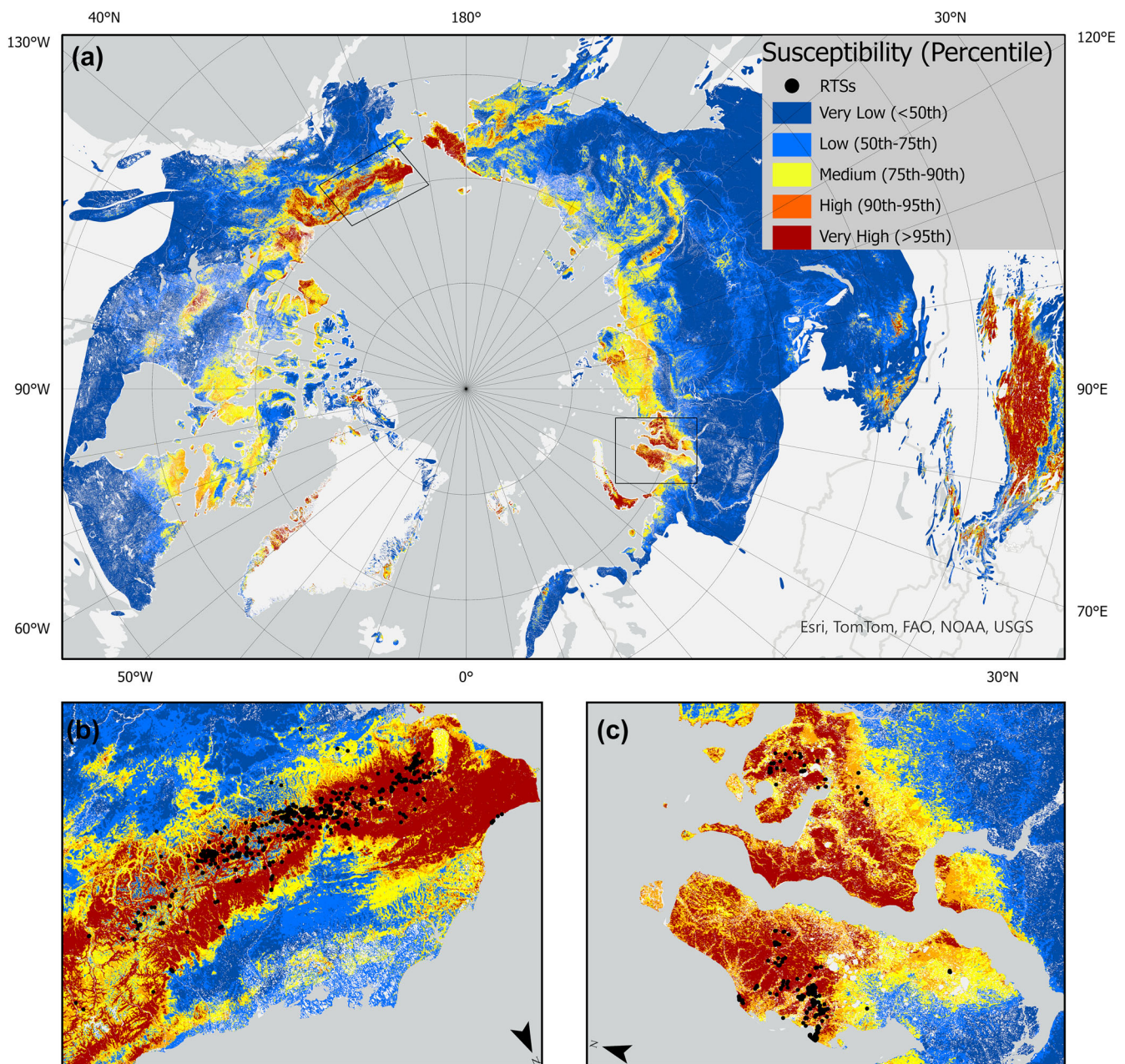


FIGURE 4 Susceptibility maps for retrogressive thaw slump (RTS) occurrences based on generalized boosting model for (a) circumpolar permafrost area, (b) northern Alaska and (c) Yamal and Gydan peninsulas. Also shown are the compiled retrogressive thaw slumps (b and c).

(e.g., Lewkowicz & Way, 2019; Nicu et al., 2023; Rudy et al., 2016; Yin et al., 2021). For example, Yin et al. (2021) reported that climatic variables, TDD and rainfall, were the two most important factors for the occurrence of permafrost hazards in the Qinghai-Tibetan Plateau. Luo et al. (2022) confirmed that the increase in the RTS occurrence in the Qinghai-Tibetan Plateau mainly occurred during the warm season in 2010 and 2016 and is likely due to high air temperatures during the thawing season. Furthermore, Kokelj, Tunnicliffe, Lacelle, Lantz, and Fraser (2015) demonstrated that an increase in rainfall accelerated slump activity in the Peel Plateau and may have been an essential factor driving increased slump activity in many parts of the Arctic and subarctic of northwestern Canada.

Although climatic factors were the most important variables of RTS occurrences in our study, the results indicated that soil properties were also central in depicting suitable conditions for occurrence. Soil dry bulk density was used to characterize the overall compactness of the soils and it ended up being an important variable in the model – second only to the climatic factors FDD, TDD and rainfall. In this study, the role of slope angle was also highlighted, and the response curve (Figure 3) showed that the suitable slopes should not exceed 20 degrees. Lacelle et al. (2015) studied the distribution of RTSs in the Richardson Mountains and concluded that RTSs were more likely to occur on ice-rich moraines with slopes of 8–12 degrees. Similarly, Rudy et al. (2016) explored the effect of terrain variables on the occurrence of permafrost hazards in two locations on Melville Island and one location on Ellesmere Island and concluded that permafrost hazards commonly occurred on slopes between 4 and 15 degrees.

Fine sediment content had a moderate importance in the models, but RTS probability showed a substantial increase with higher fine sediment contents (Figure 3). This finding is consistent with Jones, Pollard, & Jones (2019) who found that RTSs are abundant in regions with very fine-grained marine deposits, which are prone to the growth of segregation ice (Kokelj & Burn, 2005). The response curves indicated a clear optimal bulk density range (90–105 g/cm³) for suitable conditions. Typically, these kinds of values are found in organic materials, but the values here should be interpreted cautiously. This is because we also included the very low-density surface layer of the soil (0–5 cm) from the SoilGrids data, which strongly lowered the average for the used 0–200 cm interval. The predicted optimal range is argued to represent soils that are denser than organic soils but still not extremely dense, clayey soils that could limit ground ice accumulation. For example, Kokelj et al. (2017) demonstrated that thaw slumps occurred in ice-marginal hummocky moraines, but were also present in glaciofluvial, glaciolacustrine and isostatically uplifted glaciomarine deposits.

This study employed statistical modelling techniques to create the first RTS susceptibility map in the Northern Hemisphere based on available environmental datasets. The results provided information about the environmental factors that affect the susceptibility of RTS occurrence and may enable us to better understand how RTS activity responds to a changing climate and permafrost thaw at a circumpolar scale. Liu et al. (2024), highlighted that RTS activity is well connected with warming temperatures and in the Arctic is 1.5 times higher than in the Third Pole. Our susceptibility map indicated high susceptibility in many regions where previous studies have documented increased RTS activity (Kokelj et al., 2017; Leibman, Nesterova, & Altukhov, 2023; Mu et al., 2020; Segal, Lantz, & Kokelj, 2016;

Young et al., 2022). More specifically, our susceptibility map concurred with the findings of Ramage et al. (2018) that RTSs have strong preconditioning across the Yukon Coast, where their occurrence has increased by 73% between 1952 and 2011. Lewkowicz & Way (2019) pointed out that RTS initiation rates increased on Banks Island and provided evidence that continuous permafrost areas can be vulnerable to changing climatic conditions which also aligns with our results. In the Qinghai-Tibetan Plateau, RTS activity has rapidly accelerated in the ice-rich alpine permafrost regions (Luo et al., 2022; Xia et al., 2022), which showed very high susceptibility in our study (Figure 4a). Based on the predicted high susceptibilities, RTSs can be found or are expected to be found in discontinuous permafrost regions across the Qinghai-Tibetan Plateau in the future.

Our susceptibility map indicated high to very high susceptibility in the eastern, central and western Brooks Range and foothills of northern Alaska (Figure 4b), where we have observations on RTS occurrences mainly in the central part. The model could not distinguish the rocky areas with thin soils in the eastern part of Brooks Range (Wilson et al., 2015) from the environmental parameters, but it resulted in low to very low susceptibility in a large part of the Alaskan Coastal Plain, where extensive RTSs are rare due to unconsolidated and poorly consolidated surficial deposits in the area with little or no relief (Wilson et al., 2015). Furthermore, the low density of RTS occurrence in rolling, thaw-lake-dominated areas is a function of gentle topographic gradients and thaw truncation or eradication of ground ice by thermokarst during the early Holocene warm period (Burn, 1997; Murton, 2001). In Mackenzie Bay and Mackenzie Mountain foothills, our map showed high to very high susceptibility, which agrees with the findings of Young et al. (2022) that permafrost mass-wasting has increased substantially from 2004 to 2020 in these areas due to a combination of increased summer precipitation and fire disturbances. West of Great Slave Lake, our model indicated medium to high susceptibility even though there were no available observations from that area. This area also has generally very gentle slopes <3° yet the climate and soil conditions are suitable for the occurrence of RTSs or other thermokarst features (Kokelj et al., 2023). Additionally, a similar situation is in the Chukotka area, where our model provided very high susceptibility with a limited number of observations available but favourable climate conditions (TDD values 900°C-days and FDD values from 3,600 to 4,000°C-days approximately). Finally, the susceptibility map showed very high susceptibility in the Yamal and Gydan peninsulas (Figure 4c), which aligns with the used observations and results in Leibman, Nesterova, & Altukhov (2023).

Despite the fact that RTSs typically have a size of roughly 10 ha, with some exceptions reaching up to 1 km² (Nitze et al., 2021), our analysis showed that their circumpolar modelling was possible using openly available geospatial datasets with circumpolar coverage. GBM was effective at predicting RTS susceptibility in both training and spatially semi-independent evaluation datasets with an average ROC value of 0.93, which was considered excellent (Swets, 1988). The variation between modelling runs was relatively low, as indicated by the small standard deviation, even though only 10 modelling runs were performed, and as such indicative of stable model performance. TSS values were lower for both the training and evaluation datasets. The models showed high sensitivity, correctly predicting on average 92% of RTS presence observations, but the lower specificity values of 83% indicated more frequent commission errors, i.e., absences predicted as

presences (Allouche, Tsoar, & Kadmon, 2006). As a result, predicted susceptibility is likely too high over some regions with no documented RTSs.

Regardless of the high ROC and TSS values indicating the reliability of this study, there were two additional factors that affected the model performance. The first factor was the lack of available observations in some regions. Our initial aim was to compile as comprehensive a dataset as possible of available RTS observations across the Northern Hemisphere permafrost region, to facilitate the training of a model that could learn all possible environmental conditions for RTS occurrence and thus be transferable in space. However, due to unavailable data in some regions, there may be environmental conditions in which RTSs occur but were not represented by the modelling data. This can hinder model transferability to unstudied regions and cause increased prediction uncertainty (see Supplementary Material Figure S7[CV]). Owing to our aim to maximize the data used in modelling, we did not retain separate regional datasets for validation purposes. Instead, we performed the distance-based random cross-validation that allowed for using the entire circumpolar RTS compilation while also enabling spatially semi-independent evaluation datasets with which predictive performance was assessed.

It should be mentioned that the distance constraint used to separate calibration and evaluation datasets (10 km) was relatively short and might have incorporated some spatial autocorrelation that influenced the modelling and produced slightly over-optimistic evaluation statistics. However, the selected threshold was necessary to avoid losing large amounts of observations from the model training data. The evaluation results were comparable to other previous modelling studies for RTSs (Rudy et al., 2016; Yin et al., 2021) and in modelling of other permafrost and periglacial landforms more generally (e.g., rock glaciers, palsas, sorted circles, pingos, ice-wedge polygon distribution; Brenning & Trombotto, 2006; Marmion et al., 2008; Hjort et al., 2014; Azócar, Brenning, & Bodin, 2017; Karjalainen et al., 2020).

Further development of spatial RTS susceptibility models would benefit from more accurate (e.g., spatial and temporal accuracy) data on climate and ground conditions but also sedimentary history. For example, the local Quaternary history (e.g., the development of sediment layers and ground ice) was not well considered by our final model. We explored the inclusion of coarse-resolution ground ice (Brown et al., 2002) and Yedoma (Strauss et al., 2021) data, but these theoretically central determinants had a low contribution to the models. This was presumably owing to the low thematic (only a few ground ice classes) and spatial accuracy of the Brown et al. (2002) data. Consequently, new high-resolution datasets on ground ice content at the circumpolar scale would be important in the development of predictive RTS susceptibility models (Lacelle et al., 2015; Lewkowicz & Way, 2019). Time series data and data on summer climate extremes could also be important as particularly warm or wet summers contribute to the abrupt thaw of ice-rich permafrost and the development of RTSs (Kokelj, Tunnicliffe, Lacelle, Lantz, Chin, & Fraser, 2015; Lewkowicz & Way, 2019). Another potential improvement could come from the use of high-resolution satellite images and radar data, through automated RTS mapping procedures (e.g., Bernhard, Zwieback, & Hajnsek, 2022; Huang et al., 2022, 2020).

The susceptibility map produced in this study can be used for estimating or identifying geohazard potential because RTSs rapidly

degrade large volumes of ice-rich permafrost and transport sediments from slopes to downstream environments (Kokelj & Jorgenson, 2013; Lantuit et al., 2012). Mass wasting processes may influence the stability of infrastructure (Kokelj & Jorgenson, 2013; Luo et al., 2019; Hjort et al., 2022), contribute to the release of organic carbon and nutrients and the displacement of large-volume sediments that can affect aquatic ecosystems by generating alterations in the water quality of nearby lakes and streams (Kokelj & Jorgenson, 2013; Kokelj et al., 2021; Ramage et al., 2017; Lewkowicz & Way, 2019), vegetation and soils (Khomutov & Leibman, 2014; Lantz et al., 2009; Segal, Lantz, & Kokelj, 2016). Thus, the susceptibility map may provide new insights into the quantitative assessments of damage to Arctic infrastructure, risk evaluation on the sustainable development of Arctic communities and assessments of the approximately 180,000 registered cultural heritage sites in the Arctic (Andrews et al., 2016; Nicu & Fatorić, 2023). Moreover, the present circumpolar RTS susceptibility model can lay the foundation for future multi-hazard (RTS and thermo-erosion gullies and more) susceptibility models (Nicu et al., 2023) for the Arctic region.

5 | CONCLUSIONS

We compiled an unprecedented dataset of RTS observations and modelled the susceptibility of RTSs using climate, soil and topography data across the permafrost region in the Northern Hemisphere. We conclude that under the current climate, RTSs can be found across the Northern Hemisphere, from the Brooks Range in Alaska and moving towards to Yukon Coast, to Mackenzie Bay in Canada, to Banks Island, northwest of Victoria Island, along the North-western Passages to all along the northern part of the Siberian coast (Yamal, Gydan, Taymyr, Sakha and Chukotka regions) and last to Qinghai-Tibetan Plateau. Based on our susceptibility model, continuous permafrost environments with suitable thaw season conditions are highly susceptible to RTSs across the Arctic, while isolated and sporadic permafrost generally have low susceptibility. Moreover, bulk density and slope angle also showed a relatively strong contribution to the occurrences of RTS. The statistical technique used in our analysis has the potential to predict the circumpolar susceptibility for RTS occurrence using openly available geospatial datasets with good to excellent classification accuracy. Local-scale prediction accuracy is limited by the lack of circumpolar data on ground ice content and surficial geology, as well as by the uncertainties in the currently available soil property data.

AUTHOR CONTRIBUTIONS

EM, OK and JH conceptualized the research idea. EM collected the data with help from LE and LR. TL, PL, IN, ABS and AR provided data. OK led the geospatial processing with EM and JH. EM and OK performed the statistical analysis with contributions from JH. EM wrote the article with contributions from all the authors.

ACKNOWLEDGEMENTS

This study was supported by the University of Oulu and KVANTUM Institute within the program Changing Climate and the Northern Environment with the title: HYPERISK, Hybrid Modelling for improved permafrost risk assessments (2021–2024) and E.M., O.K., and

J.H. acknowledge support from the Research Council of Finland (grant no. 315519). The authors acknowledge support from Yukon Geological Survey with contribution number O68.

CONFLICT OF INTEREST STATEMENT

The authors declare that they have no competing interests.

DATA AVAILABILITY STATEMENT

The data that support the findings of this study are available from the corresponding author upon reasonable request. The susceptibility map of RTSs for the permafrost region in Northern Hemisphere is publicly available in GeoTIFF format in Zenodo: <https://doi.org/10.5281/zenodo.10688087>.

ORCID

Eirini Makopoulou  <https://orcid.org/0000-0003-1065-5345>

REFERENCES

- Aalto, J., Harrison, S. & Luoto, M. (2017) Statistical modelling predicts almost complete loss of major periglacial processes in northern Europe by 2100. *Nature Communications*, 8(1), 515. Available from: <https://doi.org/10.1038/s41467-017-00669-3>
- Aalto, J., Karjalainen, O., Hjort, J. & Luoto, M. (2018) Statistical forecasting of current and future circum-Arctic ground temperatures and active layer thickness. *Geophysical Research Letters*, 45(10), 4889–4898. Available from: <https://doi.org/10.1029/2018GL078007>
- Aalto, J. & Luoto, M. (2014) Integrating climate and local factors for geomorphological distribution models. *Earth Surface Processes and Landforms*, 39(13), 1729–1740. Available from: <https://doi.org/10.1002/esp.3554>
- Allouche, O., Tsoar, A. & Kadmon, R. (2006) Assessing the accuracy of species distribution models: prevalence, kappa and the true skill statistic (TSS). *Journal of Applied Ecology*, 43(6), 1223–1232. Available from: <https://doi.org/10.1111/j.1365-2664.2006.01214.x>
- Amatulli, G., McInerney, D., Sethi, T., Strobl, P. and Domisch, S. (2020) Geomorpho90m - global high-resolution geomorphometry layers. Distributed by OpenTopography. Available from: <https://doi.org/10.5069/G91R6NPX> [Accessed 14th November 2023].
- Andrews, T.D., Kokelj, S.V., MacKay, G., Buysse, J., Kritsch, I., Andre, A., et al. (2016) Permafrost thaw and aboriginal cultural landscapes: a GIS-based risk assessment in the Gwich'in settlement region, Yukon and Northwest Territories, Canada. *APT Bulletin*, 47, 15–22.
- Azócar, G.F., Brenning, A. & Bodin, X. (2017) Permafrost distribution modelling in the semi-arid Chilean Andes. *The Cryosphere*, 11(2), 877–890. Available from: <https://doi.org/10.5194/tc-11-877-2017>
- Bartleman, A.P., Miyanishi, K., Burn, C.R. & Cote, M.M. (2001) Development of vegetation communities in a retrogressive thaw slump near Mayo, Yukon territory: a 10-year assessment. *Arctic*, 54(2), 149–156. Available from: <https://doi.org/10.14430/arctic774>
- Bernhard, P., Zwieback, S. & Hajnsek, I. (2022) Accelerated mobilization of organic carbon from retrogressive thaw slumps on the northern Taymyr peninsula. *The Cryosphere*, 16(7), 2819–2835. Available from: <https://doi.org/10.5194/tc-16-2819-2022>
- Bernhard, P., Zwieback, S., Leinss, S. & Hajnsek, I. (2020) Mapping retrogressive thaw slumps using single-pass TanDEM-X observations. *IEEE Journal of Selected Topics in Applied Earth Observations and Remote Sensing*, 13, 3263–3280 <https://doi.org/10.1109/JSTARS.2020.3000648>
- Biskaborn, B.K., Smith, S.L., Noetzli, J., Matthes, H., Vieira, G., Streletskiy, D.A., et al. (2019) Permafrost is warming at a global scale. *Nature Communications*, 10(1), 264. Available from: <https://doi.org/10.1038/s41467-018-08240-4>
- Brenning, A. (2005) Spatial prediction models for landslide hazards: review, comparison and evaluation. *Natural Hazards and Earth System Sciences*, 5(6), 853–862. Available from: <https://doi.org/10.5194/nhess-5-853-2005>
- Brenning, A. & Trombotto, D. (2006) Logistic regression modeling of rock glacier and glacier distribution: topographic and climatic controls in the semi-arid Andes. *Geomorphology*, 81(1–2), 141–154. Available from: <https://doi.org/10.1016/j.geomorph.2006.04.003>
- Brown, J., Ferrians, O., Heginbottom, J. A. and Melnikov, E. (2002) *Circum-Arctic map of permafrost and ground-ice conditions, version 2 [data set]*. Boulder, Colorado USA. National Snow and Ice Data Center. Available from: <https://doi.org/10.7265/skbg-kf16> [Accessed 5th May 2023].
- Brown, J., Sidlauskas, F.J. and Delinski, G.F. (1997) Circum-arctic map of permafrost and ground ice conditions.
- Burn, C. & Lewkowicz, A. (1990) Canadian landform examples-retrogressive thaw slumps. *Canadian Geographic*, 34(3), 967–981. Available from: <https://doi.org/10.1111/j.1541-0064.1990.tb01092.x>
- Burn, C.R. (1997) Cryostratigraphy, paleogeography, and climate change during the early Holocene warm interval, western Arctic coast, Canada. *Canadian Journal of Earth Sciences*, 34(7), 912–925. Available from: <https://doi.org/10.1139/e17-076>
- Elia, L., Castellaro, S., Dahal, A. & Lombardo, L. (2023) Assessing multi-hazard susceptibility to cryospheric hazards: lesson learnt from an Alaskan example. *Science of the Total Environment*, 898, 2023, 165289, ISSN 0048-9697. Available from: <https://doi.org/10.1016/j.scitotenv.2023.165289>
- Elith, J., Ferrier, S., Huettmann, F. & Leathwick, J. (2005) The evaluation strip: a new and robust method for plotting predicted responses from species distribution models. *Ecological Modelling*, 186(3), 280–289. Available from: <https://doi.org/10.1016/j.ecolmodel.2004.12.007>
- Elith, J., Leathwick, J.R. & Hastie, T. (2008) A working guide to boosted regression trees. *Journal of Animal Ecology*, 77(4), 802–813. Available from: <https://doi.org/10.1111/j.1365-2656.2008.01390.x>
- ESRI. (2020) Arctic Imagery 15m TerraColor Imagery for the Arctic region. Available from: <https://arcgis.com/arcgis/0Gn9mT>
- Fraser, R.H., Kokelj, S.V., Lantz, T.C., McFarlane-Winchester, M., Olthof, I. & Lacelle, D. (2018) Climate sensitivity of high Arctic permafrost terrain demonstrated by widespread ice-wedge Thermokarst on Banks Island. *Remote Sensing*, 10(6), 954. Available from: <https://doi.org/10.3390/rs10060954>
- Goetz, J.N., Brenning, A., Petschko, H. & Leopold, P. (2015) Evaluating machine learning and statistical prediction techniques for landslide susceptibility modeling. *Computers & Geosciences*, 81, 1–11. Available from: <https://doi.org/10.1016/j.cageo.2015.04.007>
- Guisan, A., Thuiller, W. and Zimmermann, N. (2017) Habitat Suitability and Distribution Models: With Applications in R. Available from: <https://doi.org/10.1017/9781139028271>
- Hao, T., Elith, J., Lahoz-Monfort, J.J. & Guillera-Aroita, G. (2020) Testing whether ensemble modelling is advantageous for maximising predictive performance of species distribution models. *Ecography*, 43(4), 549–558. Available from: <https://doi.org/10.1111/ecog.04890>
- Harris, C., Arenson, L.U., Christiansen, H.H., Etzelmüller, B., Frauenfelder, R., Gruber, S., et al. (2009) Permafrost and climate in Europe: monitoring and modelling thermal, geomorphological and geotechnical responses. *Earth-Science Reviews*, 92(3–4), 117–171. Available from: <https://doi.org/10.1016/j.earscirev.2008.12.002>
- Hjort, J. & Luoto, M. (2011) Novel theoretical insights into geomorphic process–environment relationships using simulated response curves. *Earth Surface Processes and Landforms*, 36(3), 363–371. Available from: <https://doi.org/10.1002/esp.2048>
- Hjort, J., Streletskiy, D., Doré, G., Wu, Q., Bjella, K. & Luoto, M. (2022) Impacts of permafrost degradation on infrastructure. *Nature Reviews Earth & Environment*, 3(1), 24–38. Available from: <https://doi.org/10.1038/s43017-021-00247-8>
- Hjort, J., Ujanen, J., Parviainen, M., Tolgensbakk, J. & Etzelmüller, B. (2014) Transferability of geomorphological distribution models: evaluation using solifluction features in subarctic and Arctic regions. *Geomorphology*, 204, 165–176. Available from: <https://doi.org/10.1016/j.geomorph.2013.08.002>
- Huang, L., Lantz, T.C., Fraser, R.H., Tiampo, K.F., Willis, M.J. & Schaefer, K. (2022) Accuracy, efficiency, and transferability of a deep learning model for mapping retrogressive thaw slumps across the Canadian Arctic. *Remote Sensing*, 14(12), 2747. Available from: <https://doi.org/10.3390/rs14122747>

- Huang, L., Luo, J., Lin, Z., Niu, F. & Liu, L. (2020) Using deep learning to map retrogressive thaw slumps in the Beiluhe region (Tibetan plateau) from CubeSat images. *Remote Sensing of Environment*, 237, 111534. Available from: <https://doi.org/10.1016/j.rse.2019.111534>
- Huebner, D.C. & Bret-Harte, M.S. (2019) Microsite conditions in retrogressive thaw slumps may facilitate increased seedling recruitment in the Alaskan low Arctic. *Ecology Evolution*, 9(4), 1880–1897. Available from: <https://doi.org/10.1002/ece3.4882>
- Intergovernmental Panel on Climate Change (IPCC). (2021) Climate change 2021 – The physical science basis. Available from: <https://doi.org/10.1017/9781009157896>
- Jones, M.K.W., Pollard, W.H. & Jones, B.M. (2019) Rapid initialization of retrogressive thaw slumps in the Canadian high Arctic and their response to climate and terrain factors. *Environmental Research Letters*, 14(5), 055006. Available from: <https://doi.org/10.1088/1748-9326/ab12fd>
- Karger, D.N., Conrad, O., Böhrer, J., Kawohl, T., Kreft, H., Soria-Auza, R.W., et al. (2017) Climatologies at high resolution for the earth's land surface areas. *Scientific Data*, 4(1), 170122. Available from: <https://doi.org/10.1038/sdata.2017.122>
- Karjalainen, O., Luoto, M., Aalto, J., Etzelmüller, B., Grosse, G., Jones, B.M., et al. (2020) High potential for loss of permafrost landforms in a changing climate. *Environmental Research Letters*, 15(10), 104065. Available from: <https://doi.org/10.1088/1748-9326/abaf5>
- Khomutov, A. and Leibman, M. (2014) *Assessment of landsliding hazard in typical tundra of central Yamal, Russia*. Springer eBooks, pp. 487–492. Available from: https://doi.org/10.1007/978-3-319-04996-0_74
- Kokelj, S.V. & Burn, C.R. (2005) Near-surface ground ice in sediments of the Mackenzie Delta, Northwest Territories, Canada. *Permafrost and Periglacial Processes*, 16(3), 291–303. Available from: <https://doi.org/10.1002/ppp.537>
- Kokelj, S.V., Gingras-Hill, T., Daly, S.V., Morse, P., Wolfe, S., Rudy, A.C.A., et al. (2023) The Northwest Territories Thermokarst Mapping Collective: A northern-driven mapping collaborative toward understanding the effects of permafrost thaw. *Arctic Science*, 9(4), 886–918. Available from: <https://doi.org/10.1139/as-2023-0009>
- Kokelj, S.V. & Jorgenson, M.T. (2013) Advances in Thermokarst research. *Permafrost and Periglacial Processes*, 24(2), 108–119. Available from: <https://doi.org/10.1002/ppp.1779>
- Kokelj, S.V., Kokoszka, J., van Der Sluijs, J., Rudy, A.C., Tunnicliffe, J., Shakil, S., et al. (2021) Thaw-driven mass wasting couples slopes with downstream systems, and effects propagate through Arctic drainage networks. *The Cryosphere*, 15(7), 3059–3081. Available from: <https://doi.org/10.5194/tc-15-3059-2021>
- Kokelj, S.V., Lantz, T.C., Tunnicliffe, J., Segal, R. & Lacelle, D. (2017) Climate-driven thaw of permafrost preserved glacial landscapes, northwestern Canada. *Geology*, 45(4), 371–374. Available from: <https://doi.org/10.1130/G38626.1>
- Kokelj, S.V., Tunnicliffe, J., Lacelle, D., Lantz, T. and Fraser, R. (2015) Retrogressive thaw slumps: from slope process to the landscape sensitivity of northwestern Canada, 68e *Conférence Canadienne de Géotechnique et 7e Conférence Canadienne sur le Pergélisol*, 20 au45523 September 2015, Québec.
- Kokelj, S.V., Tunnicliffe, J., Lacelle, D., Lantz, T.C., Chin, K.S. & Fraser, R. (2015) Increased precipitation drives mega slump development and destabilization of ice-rich permafrost terrain, northwestern Canada. *Global Planetary Change*, 129, 56–68. Available from: <https://doi.org/10.1016/j.gloplacha.2015.02.008>
- Lacelle, D., Bjornson, J. & Lauriol, B. (2010) Climatic and geomorphic factors affecting contemporary (1950–2004) activity of retrogressive thaw slumps on the Aklavik plateau, Richardson Mountains, NWT, Canada. *Permafrost and Periglacial Processes*, 21(1), 1–15. Available from: <https://doi.org/10.1002/ppp.666>
- Lacelle, D., Brooker, A., Fraser, R.H. & Kokelj, S.V. (2015) Distribution and growth of thaw slumps in the Richardson Mountains–Peel plateau region, northwestern Canada. *Geomorphology*, 235, 40–51. Available from: <https://doi.org/10.1016/j.geomorph.2015.01.024>
- Lantuit, H., Pollard, W.H., Couture, N., Fritz, M., Schirrmeister, L., Meyer, H., et al. (2012) Modern and late Holocene retrogressive thaw slump activity on the Yukon coastal plain and Herschel Island, Yukon territory, Canada. *Permafrost and Periglacial Processes*, 23(1), 39–51. Available from: <https://doi.org/10.1002/ppp.1731>
- Lantz, T.C., Kokelj, S.V., Gergel, S.E. & Henry, G.H.R. (2009) Relative impacts of disturbance and temperature: persistent long-term changes in microenvironment and vegetation in retrogressive thaw slumps. *Global Change Biology*, 15(7), 1664–1675. Available from: <https://doi.org/10.1111/j.1365-2486.2009.01917.x>
- Leibman, M., Nesterova, N. & Altukhov, M. (2023) Distribution and morphology of Thermocirques in the north of West Siberia, Russia. *Geosciences*, MDPI AG. Retrieved from, 13(6), 167. Available from: <https://doi.org/10.3390/geosciences13060167>
- Leppiniemi, O.H., Karjalainen, O., Aalto, J., Luoto, M. & Hjort, J. (2023) Environmental spaces for palsas and peat plateaus are disappearing at a circumpolar scale. *The Cryosphere Discussions*, 17, 1–37.
- Lewkowicz, A.G. & Way, R.G. (2019) Extremes of summer climate trigger thousands of thermokarst landslides in a high Arctic environment. *Nature Communications*, 10(1), 1329. Available from: <https://doi.org/10.1038/s41467-019-09314-7>
- Liu, C., Berry, P.M., Dawson, T.P. & Pearson, R.G. (2005) Selecting thresholds of occurrence in the prediction of species distributions. *Ecography*, 28(3), 385–393. Available from: <https://doi.org/10.1111/j.0906-7590.2005.03957.x>
- Liu, Y., Qiu, H., Ulrich, K., Wang, N., Wang, J., Huang, C., et al. (2024) Higher temperature sensitivity of retrogressive thaw slump activity in the Arctic compared to the third pole. *Science of the Total Environment*, 914, 170007. Available from: <https://doi.org/10.1016/j.scitotenv.2024.170007>
- Luo, J., Niu, F., Lin, Z., Liu, M. & Yin, G. (2019) Recent acceleration of thaw slumping in permafrost terrain of Qinghai–Tibet plateau: an example from the Beiluhe region. *Geomorphology*, 341, 79–85, ISSN 0169-555X. Available from: <https://doi.org/10.1016/j.geomorph.2019.05.020>
- Luo, J., Niu, F., Lin, Z., Liu, M., Yin, G. & Gao, Z. (2022) Inventory and frequency of retrogressive thaw slumps in permafrost region of the Qinghai–Tibet plateau. *Geophysical Research Letters*, 49(23), e2022GL099829. Available from: <https://doi.org/10.1029/2022GL099829>
- Malone, L., Lacelle, D., Kokelj, S. & Clark, I.D. (2013) Impacts of hillslope thaw slumps on the geochemistry of permafrost catchments (Stony Creek watershed, NWT, Canada). *Chemical Geology*, 356, 38–49. Available from: <https://doi.org/10.1016/j.chemgeo.2013.07.010>
- Marmion, M., Hjort, J., Thuiller, W. & Luoto, M. (2008) A comparison of predictive methods in modelling the distribution of periglacial landforms in Finnish Lapland. *Earth Surface Processes and Landforms*, 33(14), 2241–2254. Available from: <https://doi.org/10.1002/esp.1695>
- Mekonnen, Z.A., Riley, W.J., Grant, R.F. & Romanovsky, V.E. (2021) Changes in precipitation and air temperature contribute comparably to permafrost degradation in a warmer climate. *Environmental Research Letters*, 16(2), 024008. Available from: <https://doi.org/10.1088/1748-9326/abc444>
- Moreno, M., Steger, S., Tanyas, H. & Lombardo, L. (2023) Modeling the area of co-seismic landslides via data-driven models: the Kaikōura example. *Engineering Geology*, 320, 107121. Available from: <https://doi.org/10.1016/j.enggeo.2023.107121>
- Mu, C., Shang, J., Zhang, T., Fan, C., Wang, S., Peng, X., et al. (2020) Acceleration of thaw slump during 1997–2017 in the Qilian Mountains of the northern Qinghai–Tibetan plateau. *Landslides*, 17(5), 1051–1062. Available from: <https://doi.org/10.1007/s10346-020-01344-3>
- Murton, J.B. (2001) Thermokarst sediments and sedimentary structures, Tuktoyaktuk coastlands, western Arctic Canada. *Global Planetary Change*, 28, 175–192. Available from: [https://doi.org/10.1016/S0921-8181\(00\)00072-2](https://doi.org/10.1016/S0921-8181(00)00072-2)
- Nicu, I.C., Elia, L., Rubensdotter, L., Tanyas, H. & Lombardo, L. (2023) Multi-hazard susceptibility mapping of cryospheric hazards in a high-Arctic environment: Svalbard archipelago. *Earth System Science Data*,

- 15(1), 447–464. Available from: <https://doi.org/10.5194/essd-15-447-2023>
- Nicu, I.C. and Fatorić, S. (2023) Climate change impacts on immovable cultural heritage in polar regions: A systematic bibliometric review. *Wiley Interdisciplinary Reviews: Climate Change*, e822.
- Nitze, I., Cooley, S.W., Duguay, C.R., Jones, B.M. & Grosse, G. (2020) The catastrophic thermokarst lake drainage events of 2018 in northwestern Alaska: fast-forward into the future. *The Cryosphere*, 14(12), 4279–4297. Available from: <https://doi.org/10.5194/tc-14-4279-2020>
- Nitze, I., Grosse, G., Jones, B.M., Romanovsky, V.E. & Boike, J. (2018) Remote sensing quantifies widespread abundance of permafrost region disturbances across the Arctic and subarctic. *Nature Communications*, 9(1), 5423. Available from: <https://doi.org/10.1038/s41467-018-07663-3>
- Nitze, I., Heidler, K., Barth, S. & Grosse, G. (2021) Developing and testing a deep learning approach for mapping retrogressive thaw slumps. *Remote Sensing*, 13(21), 4294. Available from: <https://doi.org/10.3390/rs13214294>
- O'Connor, M.T., Cardenas, M.B., Ferencz, S.B., Wu, Y., Neilson, B.T., Chen, J., et al. (2020) Empirical models for predicting water and heat flow properties of permafrost soils. *Geophysical Research Letters*, 47(11), e2020GL087646. Available from: <https://doi.org/10.1029/2020GL087646>
- Pastick, N.J., Jorgenson, M.T., Wylie, B.K., Nield, S.J., Johnson, K.D. & Finley, A.O. (2015) Distribution of near-surface permafrost in Alaska: estimates of present and future conditions. *Remote Sensing of Environment*, 168, 301–315. Available from: <https://doi.org/10.1016/j.rse.2015.07.019>
- Patton, A., Rathburn, S.L. & Capps, D.M. (2019) Landslide response to climate change in permafrost regions. *Geomorphology*, 340, 116–128. Available from: <https://doi.org/10.1016/j.geomorph.2019.04.029>
- Pebesma, E.J. (2018) Simple features for R: standardized support for spatial vector data. *R Journal*, 10(1), 439. Available from: <https://doi.org/10.32614/RJ-2018-009>
- Peng, X., Zhang, T., Frauenfeld, O.W., Wang, K., Luo, D., Cao, B., et al. (2018) Spatiotemporal changes in active layer thickness under contemporary and projected climate in the northern hemisphere. *Journal of Climate*, 31(1), 251–266. Available from: <https://doi.org/10.1175/JCLI-D-16-0721.1>
- Poggio, L., De Sousa, L.M., Batjes, N.H., Heuvelink, G., Kempen, B., Ribeiro, E., et al. (2021) SoilGrids 2.0: producing soil information for the globe with quantified spatial uncertainty. *The Soil*, 7(1), 217–240. Available from: <https://doi.org/10.5194/soil-7-217-2021>
- R Core Team. (2022) *R: a language and environment for statistical computing*. R Foundation for Statistical Computing, Vienna, Austria. Available from: <https://www.R-project.org/>
- Ramage, J.L., Irrgang, A.M., Morgenstern, A. & Lantuit, H. (2017) Contribution of coastal retrogressive thaw slumps to the nearshore organic carbon budget along the Yukon coast. *Biogeosciences Discussions*. Available from: <https://doi.org/10.5194/bg-2017-437>
- Ramage, J.L., Irrgang, A.M., Morgenstern, A. & Lantuit, H. (2018) Increasing coastal slump activity impacts the release of sediment and organic carbon into the Arctic Ocean. *Biogeosciences*, 15(5), 1483–1495. Available from: <https://doi.org/10.5194/bg-15-1483-2018>
- Rantanen, M., Karpechko, A.Y., Lipponen, A., Nordling, K., Hyvärinen, O., Ruosteenoja, K., et al. (2022) The Arctic has warmed nearly four times faster than the globe since 1979. *Communications Earth & Environment*, 3(1), 168. Available from: <https://doi.org/10.1038/s43247-022-00498-3>
- Roberts, D.R., Bahn, V., Ciuti, S., Boyce, M.S., Elith, J., Guillera-Aroita, G., et al. (2017) Cross-validation strategies for data with temporal, spatial, hierarchical, or phylogenetic structure. *Ecography*, 40(8), 913–929. Available from: <https://doi.org/10.1111/ecog.02881>
- Romanovsky, V.E., Smith, S.L. & Christiansen, H.H. (2010) Permafrost thermal state in the polar northern hemisphere during the international polar year 2007–2009: a synthesis. *Permafrost and Periglacial Processes*, 21(2), 106–116. Available from: <https://doi.org/10.1002/ppp.689>
- Rudy, A.C., Lamoureux, S.F., Treitz, P. & Van Ewijk, K.Y. (2016) Transferability of regional permafrost disturbance susceptibility modelling using generalized linear and generalized additive models. *Geomorphology*, 264, 95–108. Available from: <https://doi.org/10.1016/j.geomorph.2016.04.011>
- Schratz, P., Muenchow, J., Iturrutxa, E., Richter, J. & Brenning, A. (2019) Hyperparameter tuning and performance assessment of statistical and machine-learning algorithms using spatial data. *Ecological Modelling*, 406, 109–120. Available from: <https://doi.org/10.1016/j.ecolmodel.2019.06.002>
- Segal, R.A., Lantz, T.C. & Kokelj, S.V. (2016) Acceleration of thaw slump activity in glaciated landscapes of the Western Canadian Arctic. *Environmental Research Letters*, 11(3), 034025. Available from: <https://doi.org/10.1088/1748-9326/11/3/034025>
- Shangguan, W., Hengl, T., Mendes de Jesus, J., Yuan, H. & Dai, Y. (2017) Mapping the global depth to bedrock for land surface modeling. *Journal of Advances in Modeling Earth Systems*, 9(1), 65–88. Available from: <https://doi.org/10.1002/2016MS000686>
- Smith, S.L., O'Neill, H.B., Isaksen, K., Noetzi, J. & Romanovsky, V.E. (2022) The changing thermal state of permafrost. *Nature Reviews Earth & Environment*, 3(1), 10–23. Available from: <https://doi.org/10.1038/s43017-021-00240-1>
- Snyder, C.W. (2016) Evolution of global temperature over the past two million years. *Nature*, 538(7624), 226–228. Available from: <https://doi.org/10.1038/nature19798>
- Strauss, J., Laboor, S., Schirmeister, L., Fedorov, A.N., Fortier, D., Froese, D., et al. (2021) Circum-Arctic map of the Yedoma permafrost domain. *Frontiers in Earth Science*, 9, 1001. Available from: <https://doi.org/10.3389/feart.2021.758360>
- Swanson, D.K. (2014) Mapping of erosion features related to thaw of permafrost in the NPS Arctic Inventory and Monitoring Network, Alaska. *Natural Resource Data Series NPS/ARC/NRDS-2010*, 122.
- Swets, J.A. (1988) Measuring the accuracy of diagnostic systems. *Science*, 240(4857), 1285–1293. Available from: <http://www.jstor.org/stable/1701052>, <https://doi.org/10.1126/science.3287615>
- Tan, P.N. (2009) Receiver operating characteristic. *Encyclopedia of Database Systems*, 2349–2352. Available from: https://doi.org/10.1007/978-0-387-39940-9_569
- Thuiller, W., Lafourcade, B., Engler, R. & Araújo, M.B. (2009) BIOMOD—a platform for ensemble forecasting of species distributions. *Ecography*, 32(3), 369–373. Available from: <https://doi.org/10.1111/j.1600-0587.2008.05742.x>
- Turetsky, M.R., Abbott, B.W., Jones, M.C., Anthony, K.W., Olefeldt, D., Schuur, E.A., et al. (2020) Carbon release through abrupt permafrost thaw. *Nature Geoscience*, 13(2), 138–143. Available from: <https://doi.org/10.1038/s41561-019-0526-0>
- Valavi, R., Elith, J., Lahoz-Monfort, J.J. & Guillera-Aroita, G. (2021) Modelling species presence-only data with random forests. *Ecography*, 44(12), 1731–1742. Available from: <https://doi.org/10.1111/ecog.05615>
- Valavi, R., Guillera-Aroita, G., Lahoz-Monfort, J.J. & Elith, J. (2022) Predictive performance of presence-only species distribution models: a benchmark study with reproducible code. *Ecological Monographs*, 92(1), e01486. Available from: <https://doi.org/10.1002/ecm.1486>
- Wang, C., Shan, W., Guo, Y., Hu, Z. & Jiang, H. (2015) Permafrost distribution research based on remote sensing technology in northwest section of Lesser Khingan Range in China. In: *Engineering geology for society and territory-volume 1: climate change and engineering geology*. Cham: Springer International Publishing, pp. 285–290. Available from: https://doi.org/10.1007/978-3-319-09300-0_53
- Wilson, F.H., Hulst, C.P., Mull, C.G. and Karl, S.M. (2015) Geologic map of Alaska: U.S. Geological Survey Scientific Investigations Map 3340, 197 p., 2 sheets, scale 1:1,584,000. Available from: <https://doi.org/10.3133/sim3340>
- Xia, Z., Huang, L., Fan, C., Jia, S., Lin, Z., Liu, L., et al. (2022) Retrogressive thaw slumps along the Qinghai–Tibet Engineering Corridor: a comprehensive inventory and their distribution characteristics. *Earth System Science Data*, 14(9), 3875–3887. Available from: <https://doi.org/10.5194/essd-14-3875-2022>

- Yin, G., Luo, J., Niu, F., Lin, Z. & Liu, M. (2021) Machine learning-based thermokarst landslide susceptibility modeling across the permafrost region on the Qinghai-Tibet plateau. *Landslides*, 18(7), 2639–2649. Available from: <https://doi.org/10.1007/s10346-021-01669-7>
- Young, J.M., Álvarez, A., van Kokelj, S.V., Rudy, A., McPhee, A., Stoker, B.J., et al. (2022) Recent intensification (2004–2020) of permafrost mass-wasting in the Central Mackenzie Valley foothills is a legacy of past forest fire disturbances. *Geophysical Research Letters*, 49(24), Available from: <https://doi.org/10.1029/2022gl100559>
- Zhang, L., Huettmann, F., Zhang, X., Liu, S., Sun, P., Yu, Z., et al. (2019) The use of classification and regression algorithms using the random forests method with presence-only data to model species' distribution. *MethodsX*, 6, 2281–2292. Available from: <https://doi.org/10.1016/j.mex.2019.09.035>

SUPPORTING INFORMATION

Additional supporting information can be found online in the Supporting Information section at the end of this article.

How to cite this article: Makopoulou, E., Karjalainen, O., Elia, L., Blais-Stevens, A., Lantz, T., Lipovsky, P. et al. (2024) Retrogressive thaw slump susceptibility in the northern hemisphere permafrost region. *Earth Surface Processes and Landforms*, 1–13. Available from: <https://doi.org/10.1002/esp.5890>